Exchange-based two-qubit gate for singlet-triplet qubits

Matthew P. Wardrop and Andrew C. Doherty
Centre for Engineered Quantum Systems, School of Physics, The University of Sydney, Sydney NSW 2006, Australia
(Received 21 May 2014; revised manuscript received 7 July 2014; published 21 July 2014)

We analyze a simple exchange-based two-qubit gate for singlet-triplet qubits in gate-defined semiconductor quantum dots that can be implemented in a single exchange pulse. Excitations from the logical subspace are suppressed by a magnetic field gradient that causes spin-flip transitions to be non-energy-conserving. We show that the use of adiabatic pulses greatly reduces leakage processes comapred to square pulses. We also characterize the effect of charge noise on the entanglement fidelity of the gate both analytically and in simulations; demonstrating high entanglement fidelities for physically realistic experimental parameters. Specifically we find that it is possible to achieve fidelities and gate times that are comparable to single-qubit states using realistic magnetic field gradients.

DOI: 10.1103/PhysRevB.90.045418 PACS number(s): 73.21.La, 03.67.Lx

I. INTRODUCTION

Semiconductor quantum dot systems have become an increasingly promising architecture for large-scale quantum computing [1,2], growing out of the seminal work of Loss and DiVincenzo [3]. Any successful quantum computing architecture must, with high reliability and precision, be able to encode information, perform universal logical operations, generate measurable results, and be scalable to allow for large computations [4]. While various semiconductor materials have yielded promising results, including, among others, silicon [5,6] and carbon [7,8] based structures, GaAs/AlGaAs heterostructures remain very popular due to the advanced techniques developed for this material by experimenters.

The original semiconductor proposal [3] recognized the two-level spin system of an electron localized in a gate-defined semiconductor quantum dot as a natural encoding of a qubit, which is now called the Loss-DiVincenzo qubit. Two-qubit control was to be provided by exchange coupling between the dots, which has been implemented by modifying the gate voltages that define the dots [9]; and is now a matter of routine practice. Single-qubit control is more challenging [10–14], and is usually implemented using electrically driven spin resonance in the presence of magnetic field gradients that allow for individual addressing.

Various modifications to Loss-DiVincenzo qubits and their manipulation have been proposed, each trading off the relative simplicity of single electron spin qubit encoding for systems of greater redundancy, ease of implementation, and/or resilience to experimental noise. Among the most promising of these new proposals are the "singlet-triplet" qubits [15–24], which will be the focus of this paper. Another promising candidate is the exchange-only qubit [25–30], which encodes logical qubits in the spins of three electrons; allowing for full electronic control through the exchange interaction alone.

Singlet-triplet qubits encode logical information in a pair of electron spins. The logical subspace of these qubits is the two-dimensional subspace of a pair of electron spins that is not Zeeman-shifted in an applied magnetic field, making them resistant to global magnetic field fluctuations [15]. Single-qubit operations are performed using a (potentially static) magnetic field gradient and an exchange coupling between the dots. We describe these qubits in more detail in Sec. III A. Static magnetic field gradients have been demonstrated using dynamic nuclear polarization [31,32] and patterned nanomagnets[33,34]; with gradients as large as 100 mT. There have been several proposals for two-qubit operations, the realization of any being sufficient for universality of quantum computation [35]. The only two-qubit gate currently demonstrated in experiment uses capacitive coupling [21,36].

In this paper we present a proposal for an exchange-based two-qubit gate for neighboring singlet-triplet qubits that can effect high fidelity operations in a single adiabatic pulse. The use of exchange coupling has the significant advantage that gates can be fast, with gate times comparable to single-qubit operations. However, use of exchange coupling between singlet-triplet qubits typically causes spin-flip transitions that result in excursions from the qubit subspace, leading to so-called leakage errors. Such leakage errors are suppressed during our gate by a static magnetic field gradient that causes spin-flip transitions to violate energy conservation, and are further mitigated by the adiabatic pulsing of the interqubit exchange couplings. Our proposal does not depend on the details of the substrate in which the quantum dots are embedded, or the way in which the exchange coupling and magnetic field gradients are realized, allowing for novel effective fields and couplings to be used (e.g., [37,38]). In simulations incorporating physically realistic charge noise, we found that with static magnetic field gradients less than 100 mT, and gate times as short as 7 ns, our gate can perform with entanglement fidelities in excess of 99.9%. In this regime, our gate performs with similar fidelity to single qubit operations. Our study complements a similar proposal described by Klinovaja and collaborators [23], which considers pulse sequences as an alternative to adiabatic pulses for solving the problems of leakage, and focuses on spin-orbit coupling and Overhauser noise instead of charge noise. In addition, Li and collaborators [39] describe several pulse sequences which can effect two-qubit gates, and Kestner [40], Wang [41], and collaborators have developed pulse sequences which mitigate the effect of low-frequency Overhauser and charge noise. The notion of energetically suppressing leakage processes also appears in our two-qubit gate proposal [30] for the resonant exchange qubit [28,42], in which context the use of adiabatic pulses is also expected to lead to significant reduction in leakage.

Our two-qubit gate does not have some of the drawbacks of earlier proposals. The exchange-based two-qubit gate accompanying the original singlet-triplet qubit proposal [15] required a sequence of complicated exchange pulses between neighboring singlet-triplet qubits. Apart from their complexity, these sequences also required very precise timing and negligible charge noise in order to minimize leakage. Capacitive two-qubit gate proposals [21,36,43,44] have the advantage of having actually been implemented, and being applicable for more widely spaced qubits, but it has proven difficult thus far to create large charge dipoles in singlet-triplet qubits, leading to gate times an order of magnitude slower than single-qubit exchange gates [9,36]. There have been some promising proposals to strengthen capacitive interactions, such as floating gates [44]. A more fundamental limitation is that charge noise in the control voltages couples into capacitive interactions unfavorably [21]. In contrast, our proposal promises gates that can be implemented between nearest neighbors using relatively simple adiabatic pulses; with gate times comparable to single-qubit operations, and a more favorable noise scaling that allows one to trade off gate speed for less sensitivity to charge noise.

This paper is organised as follows: in Sec. II we describe a model for semiconductor quantum dot systems; in Sec. III we describe the mechanics of our two-qubit operation; in Sec. IV we introduce a model for charge noise in singlet-triplet systems; in Sec. V we analytically investigate the performance of our gate subject to this charge noise model; in Sec. VI we present the results of simulations of our two-qubit gate and compare with the results of the previous section; and in Sec. VII we discuss the significance of these results.

II. PHYSICAL MODEL

In this section we introduce the model we use to describe exchange-coupled quantum dots, which we use in the following section to explain the mechanism of our proposed two-qubit gate for singlet-triplet qubits.

We have chosen to model a system of N electrons (each isolated in a gate-defined quantum dot) with the time-dependent Heisenberg Hamiltonian:

$$H(t) = \mu \sum_{n=1}^{N} B_n(t)\sigma_z^n + \frac{1}{4}\sum_{\langle i,j\rangle} J_{ij}(t)(\boldsymbol{\sigma}^i \cdot \boldsymbol{\sigma}^j - I), \qquad (1)$$

where $\langle i,j\rangle$ indicates that the sum should only include pairs of i and j if there exists non-negligible quantum tunneling between quantum dots i and j; and $\boldsymbol{\sigma}^i$ is the vector of Pauli operators $(\sigma_x,\sigma_y,\sigma_z)$ acting on dot i. The first sum of terms describes Zeeman splitting of the spin states at each dot due to the local magnetic field $B_n(t)$, and the second describes the exchange couplings $J_{ij}(t)$ between the dots. We set $\hbar = 1$ throughout this paper.

A large external magnetic field $B_0 = \boldsymbol{B}_0^z = \frac{1}{4}\sum_n B_n$ creates a preferred orientation, which we arbitrarily label the z axis. All of the magnetic fields B_n are taken to be along this z axis, as the effects of perpendicular fields will be suppressed provided $\boldsymbol{B}_n^{\perp} \ll \boldsymbol{B}_n^z$. We will find it useful to consider the magnetic fields in the following basis: the global background magnetic field $B_0 = \frac{1}{4}\sum_n B_n$, the interqubit gradient $\Delta B = \frac{1}{2}(B_1 + B_2 - B_3 - B_4)$, and the intraqubit gradients Δ_{12} and Δ_{34} with $\Delta_{ij} = B_i - B_j$. Thus $B_1 = B_0 + \frac{1}{2}\Delta B + \frac{1}{2}\Delta_{12}$, and so on.

Computation using singlet-triplet qubits requires control of the exchange couplings $J_{ij}(t)$, which depend on the shape of the quantum dot potential wells that are in turn determined by electrode voltages that we parametrize by ε_{ij}, and so $J_{ij}(t) = J_{ij}[\varepsilon_{ij}(t)]$. The precise dependence of J_{ij} on ε_{ij} is determined by the microscopic details of experimental apparatus. In order to make quantitative statements about our proposal, in Sec. IV B we will consider a phenomenological fit to data from GaAs/AlGaAs singlet-triplet experiments.

This model can be regarded as an approximation of the more general Hubbard model with N sites, local magnetic fields $\boldsymbol{B}_n(t)$, and tunneling between sites i and j of $t_{ij}(t)$. The exchange coupling terms $J_{ij}(\boldsymbol{\sigma}\cdot\boldsymbol{\sigma} - II)$ are the second-order perturbative effect of quantum tunneling t_{ij}, with $J_{ij} = 4t_{ij}^2/E_C$, where E_C is the energy penalty associated with charging a quantum dot with two electrons. This approximation holds in the limit of weak tunneling $t_{ij} \ll E_C$.

III. LOGICAL OPERATIONS

In this section we provide an intuition for how our gate works, before describing it in detail. The key physics that underpins the operation of our gate is the same as for single-qubit exchange gates, made more complicated by the possibility of low-energy excitations from the logical subspace. We suppress these by applying a gradient magnetic field to make spin-flip transitions non-energy-conserving, as also discussed in Klinovaja *et al.* [23]. We first review single-qubit gates.

A. Single-qubit gates for singlet-triplet qubits

Singlet-triplet qubits are encoded in the spins of two electrons, each isolated in a quantum dot (such as one of the qubits in Fig. 1), and are controlled using interdot magnetic field gradients and variable exchange coupling, in the presence of a strong global magnetic field. The Hamiltonian describing such a system is that given by Eq. (1) restricted to two dots ($N = 2$).

The strong global magnetic field B_0 makes the spin basis a natural one for this system: $|\uparrow\uparrow\rangle$, $|\uparrow\downarrow\rangle$, $|\downarrow\uparrow\rangle$, and $|\downarrow\downarrow\rangle$, where the arrows indicate the $\hat{S}^z$ projection of the electrons' spin. The global field B_0 Zeeman splits the $\sum \hat{S}^z \neq 0$ states from the $\sum \hat{S}^z = 0$ states, which energetically suppresses the hyperfine interactions between the electron and semiconductor lattice nuclear spins that would otherwise cause excitations between them [9]. The singlet-triplet qubit is encoded in the two-dimensional $\sum \hat{S}^z = 0$ subspace, which is spanned by the states $\{|\uparrow\downarrow\rangle, |\downarrow\uparrow\rangle\}$. The exchange term $\frac{1}{4}J_{12}(\boldsymbol{\sigma}^1\cdot\boldsymbol{\sigma}^2 - I)$ has two eigenstates in the logical subspace: the singlet state $|S\rangle = (|\uparrow\downarrow\rangle - |\downarrow\uparrow\rangle)/\sqrt{2}$ and the $\hat{S}_z = 0$ triplet state $|T_0\rangle = (|\uparrow\downarrow\rangle + |\downarrow\uparrow\rangle)/\sqrt{2}$, which are customarily chosen to be the computational basis states (hence the name "singlet-triplet" qubit [9]).

Universal control of a qubit entails the ability to perform arbitrary rotations of Bloch vectors around the Bloch sphere, which requires two independent axes of rotation. For singlet-triplet qubits, these are provided by a static

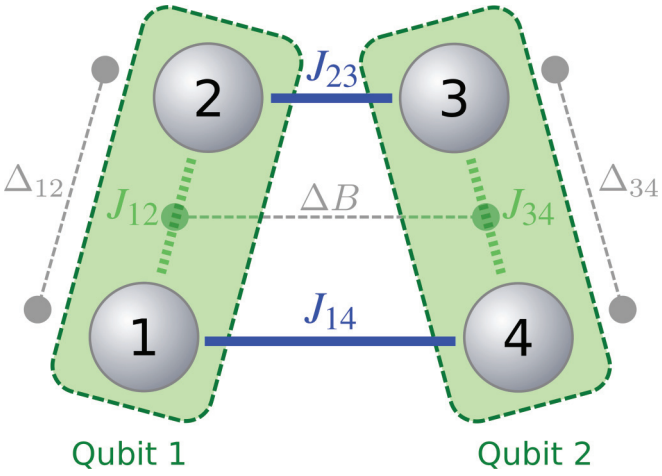

FIG. 1. (Color online) Schematic diagram of a two-singlet-triplet-qubit configuration. The four quantum dots are indexed by {1,2,3,4}, and are slanted to indicate that a specific physical arrangement is unimportant. The intraqubit exchange couplings required for single-qubit operations are shown in dashed green (J_{12} and J_{34}); and the interqubit couplings required for our two-qubit gate operation are shown in solid blue (J_{14} and J_{23}). Important magnetic field gradients are depicted by thin broken grey lines joining solid discs, and labeled with the appropriate symbols: $\Delta B = \frac{1}{2}(B_1 + B_2 - B_3 - B_4)$ and $\Delta_{ij} = B_i - B_j$.

magnetic field gradient $\Delta B = B_1 - B_2$ and a variable exchange coupling $J_{12}(t)$, as depicted in Fig. 2. In order to simplify discussion in this paper, we have chosen to orient the Bloch sphere such that the north and south poles are aligned with $|\uparrow\downarrow\rangle$ and $|\downarrow\uparrow\rangle$ respectively; and the x axis with the singlet state $|S\rangle = (|\uparrow\downarrow\rangle - |\downarrow\uparrow\rangle)/\sqrt{2}$ and the triplet state $|T_0\rangle = (|\uparrow\downarrow\rangle + |\downarrow\uparrow\rangle)/\sqrt{2}$. This choice of Bloch axes is unconventional (e.g., [9]), but allows us to describe the operation of our two-qubit gate in terms of diagonal Pauli z operators in subsequent sections. In this basis, the magnetic field gradient causes coherent phase evolution of

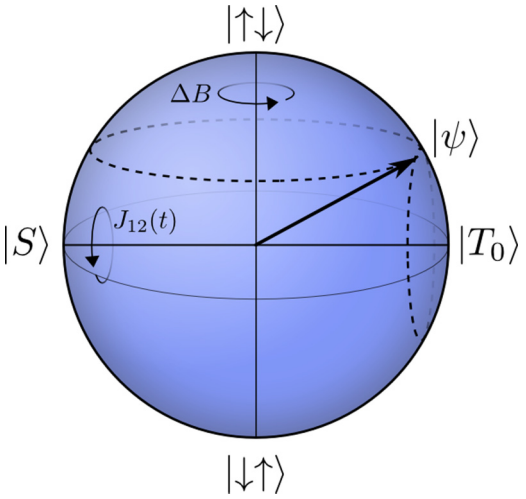

FIG. 2. (Color online) Schematic showing the alignment of the single-qubit Bloch sphere. The magnetic field gradient ΔB rotates an arbitrary qubit state $|\psi\rangle$ about the z axis of the Bloch sphere, while the exchange interaction J_{12} rotates it about the x axis.

an arbitrary superposition $|\psi\rangle = \alpha|\uparrow\downarrow\rangle + \beta|\downarrow\uparrow\rangle \mapsto \alpha|\uparrow\downarrow\rangle + \beta\exp(i\mu\Delta Bt)|\downarrow\uparrow\rangle$, which describes rotations about the z axis of the Bloch sphere. It is sufficient for this field gradient to be static, since one can keep track of the precession. The exchange operator lowers the singlet state $|S\rangle$ in energy by a controllable amount $J_{12}(t)$ compared to the triplet states $\{|\uparrow\uparrow\rangle, |T_0\rangle, |\downarrow\downarrow\rangle\}$. This causes coherent phase evolution of an arbitrary superposition $|\psi\rangle = \alpha|S\rangle + \beta|T_0\rangle \mapsto \alpha|S\rangle + \beta\exp(-i\int_0^t J_{12}(t')dt')|T_0\rangle$, which describes x axis rotations around the Bloch sphere. When $|\psi\rangle$ is an equal superposition of $|S\rangle$ and $|T_0\rangle$, these rotations are manifest as coherent oscillations between the $|\uparrow\downarrow\rangle = |T_0\rangle + |S\rangle$ and $|\downarrow\uparrow\rangle = |T_0\rangle - |S\rangle$ states. Together, these two operations can effect an arbitrary rotation in the Bloch sphere, and thus provide universal control.

To characterize single-qubit gate times for later comparison to two-qubit operations, we consider an application of a SWAP gate that has the effect of flipping the spins of the two electrons encoding the qubit state. This occurs when the qubit state $|\psi\rangle$ is rotated about the x axis of the Bloch sphere by π radians, which is when $\int_0^\tau J_{12}(t)dt = \pi$ (cf. [9]), or when gate time $\tau = \pi/J_{12\,\mathrm{avg}}$.

B. Our two-qubit exchange gate

The premise of our two-qubit gate proposal is to use exchange couplings J_{14} and J_{23} between two singlet-triplet qubits (as shown in Fig. 1) in order to perform a conditional phase gate (CPHASE) between the logical states of the two qubits.

There are four quantum dots in the combined two-qubit system, which are described by the Hamiltonian in Eq. (1) with $N = 4$. Just as for the single-qubit case, the strong background magnetic field makes the $2^4 = 16$ spin configurations a natural basis. The logical basis is the tensor product of the single-qubit subspaces: $\{|\uparrow\downarrow,\uparrow\downarrow\rangle, |\uparrow\downarrow,\downarrow\uparrow\rangle, |\downarrow\uparrow,\uparrow\downarrow\rangle, |\downarrow\uparrow,\downarrow\uparrow\rangle\}$. Unlike the single-qubit case, the logical subspace is not energetically isolated by the global magnetic field. There are two nonlogical states (called "leakage" states) which also have $\sum \hat{S}^z = 0$: $|\uparrow\uparrow,\downarrow\downarrow\rangle$ and $|\downarrow\downarrow,\uparrow\uparrow\rangle$. This makes the system susceptible to zero-energy excitations from the logical subspace. To make matters worse, such leakage transitions are actually driven from the logical states $|\uparrow\downarrow,\uparrow\downarrow\rangle$ and $|\downarrow\uparrow,\downarrow\uparrow\rangle$ by the exchange couplings J_{14} and J_{23} that are necessary for our two-qubit gate.

The addition of a magnetic field gradient ΔB between the two qubits isolates the logical subspace from the leakage states by approximately $\mu\Delta B$. In the limit that exchange couplings J_{14} and J_{23} are much less than $\mu\Delta B$, transitions from the logical subspace to the unwanted $\sum \hat{S}^z = 0$ states are energetically forbidden (and thus suppressed). We will later discuss the use of adiabatic activation of J_{ij} to further suppress leakage. Note that the field gradient must be much smaller than the applied homogeneous field $\Delta B \ll B_0$, so that B_0 remains the dominant energy scale. Since leakage from the logical subspace can in principle be made negligible by choosing small enough $J_{ij} \ll \mu\Delta B \ll \mu B_0$, we postpone further discussion of leakage until Sec. IV A, and focus on perfectly adiabatic gate operation.

During the operation of our gate, we turn off intraqubit exchange couplings J_{12} and J_{34}, before activating J_{14} and/or J_{23}. This effectively decouples the system into a new pairing of quantum dots which are described by exactly the same

Hamiltonian as singlet-triplet qubits, but which are not confined to the singlet-triplet logical subspace. In particular, notice that if the two-qubit system is initially in the logical state $|\uparrow\downarrow,\downarrow\uparrow\rangle$, then the new pairings would lead to two-quantum-dot triplet states $|\uparrow\uparrow\rangle$ and $|\downarrow\downarrow\rangle$ that previously did not correspond to logical states.

As described in Sec. III A, activating exchange coupling between dots i and j lowers the singlet energy state by J_{ij} compared to the relevant triplet states. Under J_{14} and/or J_{23}, the logical states that have singlet character under the new pairings, $|\uparrow\downarrow,\uparrow\downarrow\rangle$ and $|\downarrow\uparrow,\downarrow\uparrow\rangle$, reduce in energy by approximately $\frac{1}{2}(J_{14}+J_{23})$ compared to the other two logical states, $|\uparrow\downarrow,\downarrow\uparrow\rangle$ and $|\downarrow\uparrow,\uparrow\downarrow\rangle$. This interaction looks like a logical $\sigma_z\sigma_z$ coupling between the two singlet-triplet qubits; which is well known to generate CPHASE gates modulo single-qubit z rotations (e.g., [45]) when the phase associated with $\sigma_z\sigma_z$ has accumulated to $\pi/2$. We will show more rigorously in the following that a CPHASE gate results after a time τ such that $\int_0^\tau [J_{14}(t)+J_{23}(t)]\,dt=\pi$; or $\tau=\pi/(J_{14}+J_{23})_{\text{avg}}$. Although it appears that our gate could be twice as fast as the singlet-qubit SWAP gate (see Sec. III A), $[\sum J_{ij}]_{\text{avg}}$ is likely to be at least halved by the adiabatic pulses that are required for high fidelity operation (discussed in Sec. IV). For a more experimentally achievable linear arrangement ($J_{23}=J$, $J_{14}=0$) using an adiabatic pulse, our gate would have operation times of roughly twice that of a single-qubit SWAP gate with comparable fidelity.

We can formalize this argument by appealing to perturbation theory to further motivate the $\sigma_z\sigma_z$ coupling between the qubits. Since $J_{14}+J_{23}\ll B_0$, we can consider the exchange-coupling terms (V) to be a perturbation to the Zeeman splitting terms (H_0) of the Hamiltonian in Eq. (1). The first-order perturbed Hamiltonian will then be $H^1=H_0+PVP$, where P is a projector onto the spin basis; and hence only the diagonal components of V can affect the eigenstates of the Hamiltonian at first order. The exchange-coupling operators are of the form $\boldsymbol{\sigma}\cdot\boldsymbol{\sigma}=\sigma_x\sigma_x+\sigma_y\sigma_y+\sigma_z\sigma_z$ (identity operators omitted), and so only the $\sigma_z\sigma_z$ terms will contribute, which when projected onto the logical subspace looks like a logical $\sigma_z\sigma_z$ interaction. The $\sigma_x\sigma_x$ and $\sigma_y\sigma_y$ components give rise to corrections at higher orders of perturbation theory, which nevertheless turn out to be correctable using single-qubit phase gates.

Due to the simplicity of the model, we can in fact solve the system exactly for the eigenvalues and eigenstates by breaking the system down into a series of two-level systems, for example, for $J_{14}\neq 0$, the two-level system of $|\uparrow\downarrow,\uparrow\downarrow\rangle$ and $|\downarrow\downarrow,\uparrow\uparrow\rangle$. The energies for all eigenstates are tabulated in the Supplemental Material [46]. Since we are principally interested in the dynamics of the logical subspace, we restrict our attention to the states which adiabatically transform to the logical basis $\{|\uparrow\downarrow,\uparrow\downarrow\rangle,|\uparrow\downarrow,\downarrow\uparrow\rangle,|\downarrow\uparrow,\uparrow\downarrow\rangle,|\downarrow\uparrow,\downarrow\uparrow\rangle\}$ which we label $\{|1\rangle|1\rangle,|1\rangle|0\rangle,|0\rangle|1\rangle,|0\rangle|0\rangle\}$ respectively. We can then write a Hamiltonian, termed the "effective" Hamiltonian, that reproduces the instantaneous energy spectrum. Written in terms of effective Pauli operators $\tilde{\sigma}_z^i$ for qubit i, e.g., $\tilde{\sigma}_z^1=(|1\rangle\langle 1|-|0\rangle\langle 0|)\otimes I$, the resulting effective Hamiltonian is

$$H_{\text{eff}}=(\mu\Delta_{12}+\bar{B})\tilde{\sigma}_z^1+(\mu\Delta_{34}+\bar{B})\tilde{\sigma}_z^2 +\tfrac{1}{4}(J_{14}+J_{23})\big(\tilde{\sigma}_z^1\tilde{\sigma}_z^2-II\big), \quad (2)$$

with $\Delta_{ij}=B_i-B_j$ and $\bar{B}$ an effective global intraqubit magnetic field that depends on J_{ij} and the magnetic field gradients between each pair of dots. For the precise form of $\bar{B}$, refer to the Supplemental Material.

The effective Hamiltonian in Eq. (2) can be used to calculate the dynamical two-qubit phase accrued by adiabatic evolution of our gate; in which case our gate will perform a perfect CPHASE gate using a single exchange-coupling pulse in a time $\tau=\pi/(J_{14}+J_{23})_{\text{avg}}$ modulo known correctable single-qubit gates. One can either keep track of the single-qubit errors described by this Hamiltonian and later correct them after one or several gate operations, or correct them during the gate operation by various pulse sequences [23].

IV. SOURCES OF ERROR

Our proposed two-qubit gate will suffer from two main sources of error: leakage and environmental noise. Leakage from the logical subspace will occur due to excitations to the the nonlogical $\sum\hat{S}^z=0$ states during the course of our gate, which we suppress in our proposal using a magnetic field gradient and adiabatic exchange pulses. While the basic mechanics of our gate are agnostic about the details of implementation, the nature of environmental noise depends very much on these details. In order to make quantitative predictions about the performance of our gate, we have chosen to mimic the noisy environment of GaAs/AlGaAs semiconductor systems. In these systems, we anticipate that charge fluctuations are likely to be the largest source of environmental noise; as was observed in single qubit singlet-triplet exchange experiments [24]. As a result, in this work we neglect the Overhauser field due to the bath of nuclear spins in the semiconductor lattice, which should be less significant than charge noise over the time scale of a single gate, and which can in any case be suppressed, for example, by nuclear state preparation [31,47]. We also neglect the influence of spin-flip processes arising from spin-orbit coupling [23], which have been shown to occur on millisecond time scales [16,48] rather than the nanosecond time scales in which we are interested.

A. Leakage

We define leakage ($\mathcal{L}$) to be the probability that the state of the system, if measured, would not be in the logical subspace: $\mathcal{L}=1-\langle\psi|P|\psi\rangle$, where ψ is the state of the system, and P is the projector onto the logical subspace. In the analysis of our two-qubit gate in Sec. III B, we restricted the domain of attention to the logical subspace, explicitly neglecting leakage. Without spin-orbit coupling, leakage can only occur to other states in the $\sum\hat{S}^z=0$ subspace. Although leakage to the off-subspace states $\{|\uparrow\uparrow,\downarrow\downarrow\rangle,|\downarrow\downarrow,\uparrow\uparrow\rangle\}$ is suppressed by the energy gap $\mu\Delta B$ introduced by ΔB, if the exchange coupling terms are too quickly varied, diabatic transitions will still occur and result in leakage probability oscillations with frequency $\sim\mu\Delta B/h$; as seen for the square (nonadiabatic) profile in Fig. 3(b). Since the leakage is periodically returning to zero, it is in principle possible to minimize leakage by using precise timing of the gate in a manner similar to Levy's original proposal [15]. However, this only works in the absence of

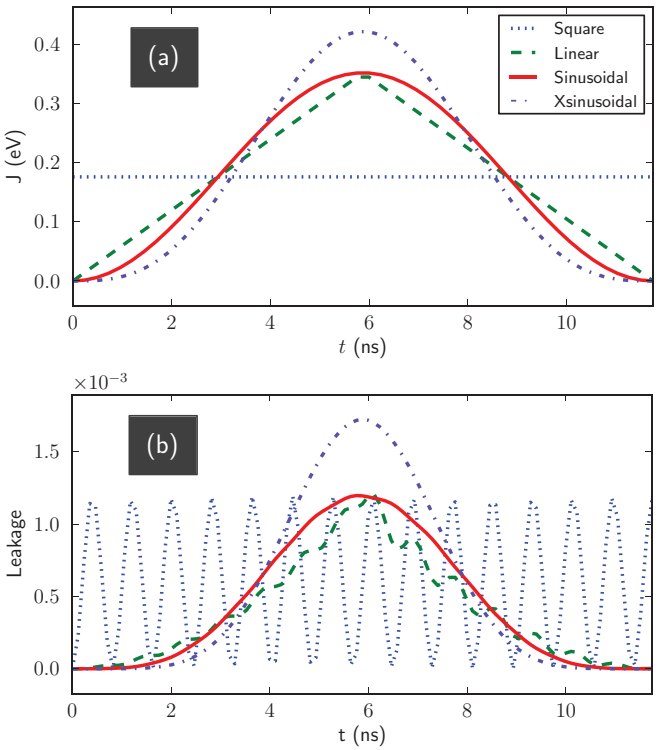

FIG. 3. (Color online) (a) The square, linear, sinusoidal, and xsinusoidal adiabatic pulse profiles discussed in the text. Amplitudes are chosen to preserve gate operation time, and hence the average value of J. We have here chosen $J_{\rm avg} = 0.18\ \mu$eV, which corresponds to a gate time of roughly 11.5 ns. (b) Leakage from the logical subspace during the operation of the gate for each of the square, linear, sinusoidal, and xsinusoidal pulses in (a). Note that the use of adiabatic profiles can significantly reduce leakage errors at the end of the gate operation.

other sources of noise, and is in practice very difficult in any case, and we suggest that the suppression of leakage using adiabatic pulses is substantially more robust.

An adiabatic pulse is one that turns on slowly and smoothly enough that the system remains in an instantaneous eigenstate. The rate at which a pulse can be turned on while remaining adiabatic depends on the energy gap between the occupied eigenstates and their neighbors. In our case, two of the four logical states $\{|\uparrow\downarrow,\uparrow\downarrow\rangle,|\downarrow\uparrow,\downarrow\uparrow\rangle\}$ can leak to the states $\{|\uparrow\uparrow,\downarrow\downarrow\rangle,|\downarrow\downarrow,\uparrow\uparrow\rangle\}$, which are separated in energy by approximately $\mu\Delta B$.

While a pulse can never be perfectly adiabatic, even a very simple adiabatic pulse can greatly improve gate performance. In this paper, we have chosen to demonstrate the behavior of adiabatic pulses using three representatives: linear, sinusoidal, and "xsinusoidal," which we compared to the nonadiabatic square pulse, as defined below:

$$J_{\rm sq}(t) = J_{\rm avg} = \frac{\pi}{\tau}, \quad J_{\rm lin}(t) = 2J_{\rm avg}\left(1 - \left|\frac{2t}{\tau} - 1\right|\right),$$

$$J_{\rm sin}(t) = J_{\rm avg}\left[1 - \cos\left(\frac{2\pi t}{\tau}\right)\right],$$

$$J_{\rm xsin}(t) = J_{\rm avg}\frac{6\pi^2}{(\pi^2+3)}\frac{t(\tau-t)}{\tau^2}\left[1 - \cos\left(\frac{2\pi t}{\tau}\right)\right],$$

each of which is depicted in Fig. 3(a). For ease of comparison, each profile has been normalized such that for any given gate time τ the area is the same as a square pulse of coupling strength $J_{\rm avg} = \pi/\tau$, which in turn will have an area π in order to enact our gate (see Sec. III B). The benefits of using an adiabatic pulse are evident in Fig. 3(b), in which leakage is reduced by several orders of magnitude at the end of the gate for all adiabatic pulse profiles.

It is possible to calculate corrections to the adiabatic approximation that provide analytic estimates of the leakage for different pulses. We used the adiabatic perturbation theory (APT) of de Grandi *et al.* [49], which predicts that the leakage probability scales with the lowest-order derivative of the adiabatic pulse that is discontinuous. There will always be a discontinuity at some differential order for $t = 0$ and $t = \tau$, and for the linear case, for $t = \tau/2$. The adiabatic pulses selected for this paper were chosen such that each profile had increasing order at which the discontinuities occurred; and in this sense are representatives of a much larger family of adiabatic pulses. Note too that we have avoided continuous profiles that are not smooth, such as adiabatic ramps to a plateau, as the reductions in adiabaticity from discontinuities would accumulate and one can always generate a pulse with the same gate time which performs better. For example, while we have included the linear ramp because of its simplicity, a better choice would have been the parabola $-J_{\rm avg}\frac{6\pi}{\tau^3}t(t-\tau)$; which would have avoided the larger leakage oscillations after $t = \tau/2$ visible in Fig. 3(b). The corrections arising from APT describe the amplitude and frequency of leakage oscillations, like those seen in Fig. 3(b). It is reasonable to assume that the experimenter will not have fine-grained temporal control due to noise and/or apparatus limitations, in which case one wants to make the conservative assumption that the gate concludes at a peak in these oscillations. Following de Grandi *et al.* [49], we calculate such a worst-case leakage probability for each of these pulses, as shown in Table I. These upper bounds are compared to data from our simulations in Fig. 4, showing reasonable agreement. As J approaches $\mu\Delta B$ in this plot, the energy gap between the logical subspace and the other $\sum \hat{S}^z = 0$ states closes, causing the evolution of the system to become strongly diabatic and resulting in a saturated leakage of 0.5 for all of the profiles (0.5 because only two of the four logical states experience leakage from the logical subspace under exchange). From these results, we derive a pattern whereby the maximum leakage for a symmetric pulse with fixed area $J_{\rm avg}\tau = \pi$ with first discontinuity at order q will

TABLE I. Maximum leakage error as calculated from adiabatic perturbation theory along the lines of de Grandi *et al.* [49] for our selection of adiabatic pulse profiles. The order of discontinuity refers to the lowest differential order (with respect to time) at which the relevant pulse exhibits a discontinuity.

Profile	Order of discontinuity	Maximum leakage
Square	0	$\propto J_{\rm avg}^2$ [for fixed ΔB]
Linear	1	$\frac{32}{\pi^2}(J_{\rm avg}/\mu\Delta B)^4$
Sinusoidal	2	$16(J_{\rm avg}/\mu\Delta B)^6$
Xsinusoidal	3	$\frac{12^4\pi^2}{4(\pi^2+3)^2}(J_{\rm avg}/\mu\Delta B)^8$

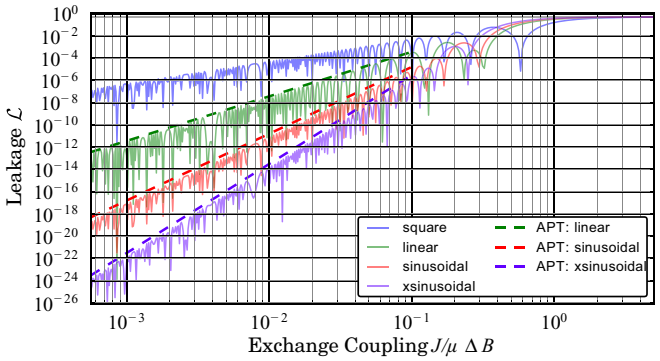

FIG. 4. (Color online) A log-log plot of leakage immediately after a gate operation as a function of $J/\mu\Delta B$. Upper bound predictions from adiabatic perturbation theory (dashed lines) are compared to data from simulations (solid traces) for the square (blue), linear (green), sinusoidal (red), and xsinusoidal (purple) adiabatic pulses, demonstrating reasonable agreement.

scale as $(J_{\text{avg}}/\mu\Delta B)^{2(q+1)}$. The implication of this scaling is that, for any given adiabatic pulse profile, the ratio of $J/\mu\Delta B$ gives a measure for the adiabaticity of the adiabatic pulse.

For the rest of this paper, we assume the use of a sinusoidal adiabatic pulse to minimize leakage. We chose the sinusoidal pulse because of its narrow bandwidth (which may make it more straightforward to generate in the laboratory) and because it boasts leakage suppression comparable with the best in the domain likely to be of most interest ($J/\mu\Delta B \approx 0.1$).

B. Charge noise

Charge noise is the result of uncontrolled electromagnetic fields coupling into the control voltages ε_{ij} of the gates defining the quantum dots, which in turn adds noise to the exchange couplings J_{ij} of Eq. (1). In this section, we describe our model for charge noise and discuss its effect on our two-qubit gate.

Since charge noise manifests itself in the control voltages ε_{ij} rather than in J_{ij} directly, we must find an ansatz for $J_{ij}(\varepsilon_{ij})$. This is very difficult to do theoretically, and so we model J's dependence phenomenologically on the basis of known experimental results on single singlet-triplet qubits (recall that singlet-triplet qubits share the same mechanism as our two-qubit gate). In several GaAs singlet-triplet qubit experiments [9,24,31], an exponential ansatz $J(\varepsilon) = J_0 \exp(\varepsilon/\varepsilon_D)$ with free parameters J_0 and ε_D has been found to be a good phenomenological fit to experimental data over a wide range of interesting values of ε_{ij}, and so we adopt it in this work. A more complicated ansatz emerges from perturbation theory [20], but due to complex interactions of the electrons with the lattice in GaAs experiments, it is not clear whether this ansatz is actually a better description.

While the noise spectrum of ε_{ij} is difficult to predict theoretically, experimental results [24] suggest that the spectrum is reasonably well approximated by a combination of low-frequency pseudostatic components $\bar{\varepsilon}_{ij}$ that do not vary significantly during the gate, and high-frequency white-noise components $\tilde{\varepsilon}_{ij}$ that do. We introduce a notation $\hat{\varepsilon}_{ij}$ to refer to the experimentally achieved control voltage, which includes noise atop the theoretically desired value ε_{ij}, i.e., $\hat{\varepsilon}_{ij} = \varepsilon_{ij} + \bar{\varepsilon}_{ij} + \tilde{\varepsilon}_{ij}$. (Dial and collaborators [24] also considered a power-law charge noise spectrum which had some advantages over this model, but we do not expect this distinction to qualitatively affect our analysis of the gate, and our simpler two-component noise spectrum allows for more straightforward analytical analyses of gate fidelities.)

We model the pseudostatic noise component $\bar{\varepsilon}_{ij}$ to be a random variable normally distributed about zero. These low-frequency components give rise to a Gaussian decay in coherence, with a relaxation time of $T_2^* = \sqrt{2}(\sigma_{\bar{\varepsilon}}|\frac{dJ}{d\varepsilon}|)^{-1}$, that is reversible using spin-echo pulses similar to those used in NMR. The standard deviation of $\bar{\varepsilon}$ ($\sigma_{\bar{\varepsilon}}$) can be determined by fitting T_2^* times from free induction decay simulations of singlet-triplet qubits to experimentally measured values. The effect of pseudostatic noise on our gate is to shift the average exchange coupling J_{avg} for the gate, causing the two-qubit phase $\int_0^\tau \{J_{14}[\hat{\varepsilon}_{14}(t)] + J_{23}[\hat{\varepsilon}_{23}(t)]\}dt$ to deviate from its ideal value of π. With our choice of ansatz for J, we find that for any sampled value of $\bar{\varepsilon}$ the two-qubit phase scales like $\pi \exp(\bar{\varepsilon}/\varepsilon_D)$. This provides the intuition that pseudostatic noise causes an under- or overaccrual of two-qubit phase that is approximately independent of gate time.

The high-frequency noise component $\tilde{\varepsilon}_{ij}$ is modelled as Gaussian white noise with mean zero, which means that it is δ correlated $\langle\tilde{\varepsilon}_{ij}(t_1)\tilde{\varepsilon}_{ij}(t_2)\rangle = D_{ij}\delta(t_1 - t_2)$, where D_{ij} is the spectral density of charge fluctuations. The first-order correction to the exchange terms in Eq. (1) due to high-frequency noise is $(dJ_{ij}/d\varepsilon_{ij})|_{\varepsilon_{ij}}\tilde{\varepsilon}_{ij}(\boldsymbol{\sigma}_i \cdot \boldsymbol{\sigma}_j - II)$. Standard methods can be used to describe the average evolution of the system in this kind of white noise in terms of a master equation [50]. The resulting Lindblad master equation for the system state ρ is found to be

$$\dot{\rho} = -i[H,\rho] + \sum_{\langle i,j\rangle} D_{ij}|dJ_{ij}/d\varepsilon_{ij}|^2\mathcal{D}[\boldsymbol{\sigma}_i \cdot \boldsymbol{\sigma}_j], \qquad (3)$$

where $\mathcal{D}[O] = O^\dagger\rho O - \frac{1}{2}(\rho O^\dagger O + O^\dagger O\rho)$ is the Lindblad superoperator for some operator O. This model describes an irreversible exponential decay in coherence, with a relaxation time of $T_2 = (8D|\frac{dJ}{d\varepsilon}|^2)^{-1}$. The spectral density of charge fluctuations D_{ij} can be determined by fitting the results of simulations to experimental T_2 relaxation times, for example, in Hahn echo experiments.

While this model of charge noise is very simple, we believe it captures the essential details of the noise to which our gate is likely to be most subjected in GaAs semiconductor systems. The model has the nice feature of being completely specified by experimental measurements of T_2 and T_2^*. An alternative would be to perform simulations with various specified power-law noise spectra, for example, $1/f$ noise [51]; however, as noted above, we would not expect qualitatively different results from this approach, at least for the performance of a single gate operation.

V. QUANTIFYING GATE PERFORMANCE

We would like to be able to say something about the performance of our two-qubit gate and its resilience against the sources of error introduced in the previous section, which requires us to have a measure of the gate's performance. While

we have already used leakage as a performance indicator in Sec. IV A, it neither characterizes the behavior of the gate on the logical subspace nor includes the effects of charge noise, and so low leakage does not imply that the desired logical operations have actually occurred. We therefore choose to quantify the performance of our gate by comparing the state of the two-qubit system to some computed ideal state using the entanglement fidelity [52]. The entanglement fidelity is designed to determine whether a gate is accurate for all possible inputs and whether it preserves any initial entanglement with the rest of an imagined quantum computer. It is defined in terms of a thought experiment in which one wants to enact an ideal gate $\bar{U}$ on one half of a maximally entangled state $|\Psi_0\rangle = \frac{1}{\sqrt{d}}\sum_i |\psi_i\rangle \otimes |\psi_i\rangle$ (where d is the number of logical states, and $d = 4$ for a two-qubit gate) to yield $|\bar{\Psi}\rangle = (\bar{U} \otimes I)|\Psi_0\rangle$. If instead we succeed only in performing U, then we yield $|\Psi\rangle = (U \otimes I)|\Psi_0\rangle$. The entanglement fidelity of U is then just the fidelity between these two states:

$$\mathcal{F} = |\langle\bar{\Psi}|\Psi\rangle|^2.$$

The entanglement fidelity is 1 if and only if the gate is perfectly implemented, and is less than 1 for all other operations, with lower values reflecting less accurate implementations of the gate. Among the attractive features of the entanglement fidelity is its simplicity and its close relationship with other measures of gate performance, such as average fidelity [53,54]. Notice that our measure of fidelity assumes that the initial state of the computation is in the logical subspace (and hence $d = 4$, rather than $d = 6$). Leakage from the logical subspace will result in $|\Psi\rangle$ living in a larger space, and hence a reduction of entanglement fidelity. The entanglement fidelity can be trivially extended to describe the fidelity of nonunitary (noisy) implementations of the gate.

We are interested only in the performance of the two-qubit component of the implemented unitary. Since universal single-qubit operations are already possible (see Sec. III A) and well characterized [9], we need only a nontrivial two-qubit gate to generate a universal set of gates for quantum computation [35]. Thus, while in practice our protocol produces a CPHASE gate along with some known single-qubit rotations (as described in Sec. III B), it would not be necessary in some experimental implementations to correct them immediately after each gate application, and if it were, these gates can be echoed away by a protocol such as the one in Klinovaja *et al.* [23]. Consequently, we compute the entanglement fidelity of our gate assuming that the optimal single qubit corrections have been perfectly applied. In practice this means that we compare our gate to a constructed ideal unitary $\bar{U}$ that maintains the ideal two-qubit phase while also including whatever single qubit z rotations we find in the simulation of our gate. This corresponds to an ansatz $\bar{U} = e^{i\phi_{II}} e^{i\phi_{ZI}\tilde{\sigma}_z^1} e^{i\phi_{IZ}\tilde{\sigma}_z^2} e^{i\phi_{ZZ}\tilde{\sigma}_z^1\tilde{\sigma}_z^2}$ with global and single-qubit phases ϕ_{II}, ϕ_{IZ}, and ϕ_{ZI} extracted from simulations, and the two-qubit phase ϕ_{ZZ} set to π. There are some subtleties to this process which we discuss in the Supplemental Material [46].

The simplicity of our two-singlet-triplet-qubit model allows us to gain some intuition about the entanglement fidelity by considering the analytic solution for fidelity in terms of the leakage at the end of the gate $\mathcal{L}_0$ and the parameter $\Delta = \phi_{ZZ} - \bar{\phi}_{ZZ}$, where ϕ_{ZZ} and $\bar{\phi}_{ZZ} = \pi$ are the extracted and ideal two qubit phases respectively. Note that Δ characterizes any under- or overaccrual of two-qubit phase acquired during the gate operation. We show in the Supplemental Material [46] that the entanglement fidelity $\mathcal{F}$ at the end of the gate is

$$\mathcal{F} = \tfrac{1}{2}(1 + \sqrt{1 - 2\mathcal{L}_0}\cos(2\Delta) - \mathcal{L}_0) \tag{4}$$

$$= 1 - \mathcal{L}_0 - \Delta^2 + \mathcal{O}(\mathcal{L}_0^2) + \mathcal{O}(\mathcal{L}_0\Delta^2) + \mathcal{O}(\Delta^4). \tag{5}$$

Perfect gate implementations will have $\Delta = 0$, whereas in the presence of charge noise it will assume nonzero values since $\phi_{ZZ} \simeq \int_0^\tau [J_{14}(t) + J_{23}(t)]\,dt$.

Our charge noise model of Sec. IV B allows us to make some more quantitative statements about Δ. Consider a square pulse for simplicity (adiabatic pulses are not expected to lead to qualitatively different results) with first-order noise perturbations, $J(t) = J_{\text{avg}} + (\bar{\varepsilon} + \tilde{\varepsilon})(dJ/d\varepsilon)|_{J(\varepsilon)=J_{\text{avg}}}$, where $\bar{\varepsilon}$ and $\tilde{\varepsilon}$ are the pseudostatic and high-frequency potential fluctuations caused by charge noise (see Sec. IV B). The phase error Δ is then

$$\Delta = \frac{\pi}{J_{\text{avg}}}\left.\frac{dJ}{d\varepsilon}\right|_{J=J_{\text{avg}}} (\bar{\varepsilon} + \tilde{\varepsilon})_{\text{avg}},$$

where $(\bar{\varepsilon} + \tilde{\varepsilon})_{\text{avg}} = \int_0^\tau [(\bar{\varepsilon} + \tilde{\varepsilon})/\tau]\,dt$ is the average charge fluctuation during the operation of the gate. Our noise model posits that $\bar{\varepsilon}$ and $\tilde{\varepsilon}$ are both independent and Gaussian distributed, which allows us to easily calculate the statistical properties of $(\bar{\varepsilon} + \tilde{\varepsilon})_{\text{avg}}$: $\langle(\bar{\varepsilon} + \tilde{\varepsilon})_{\text{avg}}\rangle = 0$ and $\langle(\bar{\varepsilon} + \tilde{\varepsilon})_{\text{avg}}^2\rangle = \sigma_{\bar{\varepsilon}}^2 + D/\tau$. While different charge spectra beyond our model would lead to different time dependencies for $\langle(\bar{\varepsilon} + \tilde{\varepsilon})_{\text{avg}}^2\rangle$, it would always be qualitatively true that nonpseudostatic noise averages out over long enough time scales. This implies the statistical properties of Δ:

$$\langle\Delta\rangle = 0,$$

$$\langle\Delta^2\rangle = \frac{\pi^2}{J_{\text{avg}}^2}\left.\frac{dJ}{d\varepsilon}\right|_{J=J_{\text{avg}}}^2 \left(\sigma_{\bar{\varepsilon}}^2 + D/\tau\right).$$

If we further assume the exponential ansatz $J \simeq J_0\exp(\varepsilon/\varepsilon_D)$ we obtain a particularly simple estimate of the expected entanglement fidelity $\langle\mathcal{F}\rangle$:

$$\langle\mathcal{F}\rangle \simeq 1 - \mathcal{L}_0 - \pi^2\frac{\sigma_{\bar{\varepsilon}}^2 + D/\tau}{\varepsilon_D^2}. \tag{6}$$

This formula affords us the important intuition that one is in principle able to maximize the fidelity of our gate by choosing sufficiently long gate times, at which point fidelity will be limited by a pseudostatic noise floor that also determines the fidelity of single-qubit operations. This is evident because both leakage and the effect of high-frequency noise are monotonically decreasing functions of the choice of gate time, and pseudostatic noise contributions are constant. The leakage $\mathcal{L}_0$ due to the pulse scales as $(\tau\Delta B)^{-c}$ for some c that depends on the adiabaticity of the pulse (as shown in Sec. IV A). Additional leakage contributions arise from high-frequency noise, at a rate $4D|dJ/d\varepsilon|^2$ predicted by the master equation (3), and hence a contribution to $\mathcal{L}_0$ proportional to $D/(\tau\varepsilon_D^2)$. Since all sources of fidelity dimunition apart from pseudostatic noise decrease

TABLE II. Model parameters kept constant while exploring J and ΔB. The global magnetic field is nominal. The noise parameters $\sigma_{\bar{\varepsilon}}$ and D were calibrated by respectively matching somewhat typical values of T_2^* and T_2 from experiment [24]. The parameters for the exponential ansatz $J(\varepsilon) = J_0 \exp(\varepsilon/\varepsilon_D)$ were chosen to roughly match the experimental results of Dial and collaborators [24].

Parameter	Value
Magnetic field:	
B_0	200 mT
Noise:	
$\sigma_{\bar{\varepsilon}}$	10.3 μV
D	100 μV^2 ns
Exponential ansatz:	
J_0	-82.7 μeV ($\approx$20 GHz)
ε_D	0.35 mV

as gate time increases, pseudostatic noise will dominate at sufficiently long gate times, after which the fidelity becomes roughly independent of gate time. In the limit that leakage is no longer the dominant noise contribution, Eq. (6) reduces to the fidelity relation for a single-qubit gate, implying that our gate would operate with essentially identical fidelity as single-qubit operations.

Although we have largely neglected the effects of Overhauser field fluctuations on our simulations, since they are expected to be less significant than charge noise in the usual regime of operation, it would be straightforward to include them in this kind of analysis. The main effect of these fluctuations is to implement random single-qubit unitaries during the gate, which would result in a reduction of gate fidelity proportional to the variance of the field fluctuation.

VI. SIMULATIONS

We are left now only to demonstrate the performance of our two-singlet-triplet gate in simulations. For the purposes of this section, we integrate the time-dependent Heisenberg Hamiltonian (with and without the Lindblad terms) as described in Eqs. (1) and (3). One might worry that the weak tunneling approximation described in Sec. II might lead to appreciable errors, but simulations of a full Hubbard model generated indistinguishable results in all of our tests. We have chosen to consider a case where $J_{14} = 0$, and henceforth $J = J_{23}$, because we expect a linear arrangement of quantum dots to be more accessible to experimental implementation. Simulating a square configuration is a trivial extension that does not alter the physics; indeed it improves the gate speed for any given leakage error, and reduces the complexity of the unwanted single-qubit gates (refer to the Supplemental Material for more information [46]). For reasons mentioned in Sec. IV A, we have chosen to use the sinusoidal adiabatic pulse in these simulations.

All of the parameters used in these simulations have been chosen with current experiments in mind. The average background magnetic field B_0 is maintained as the dominant

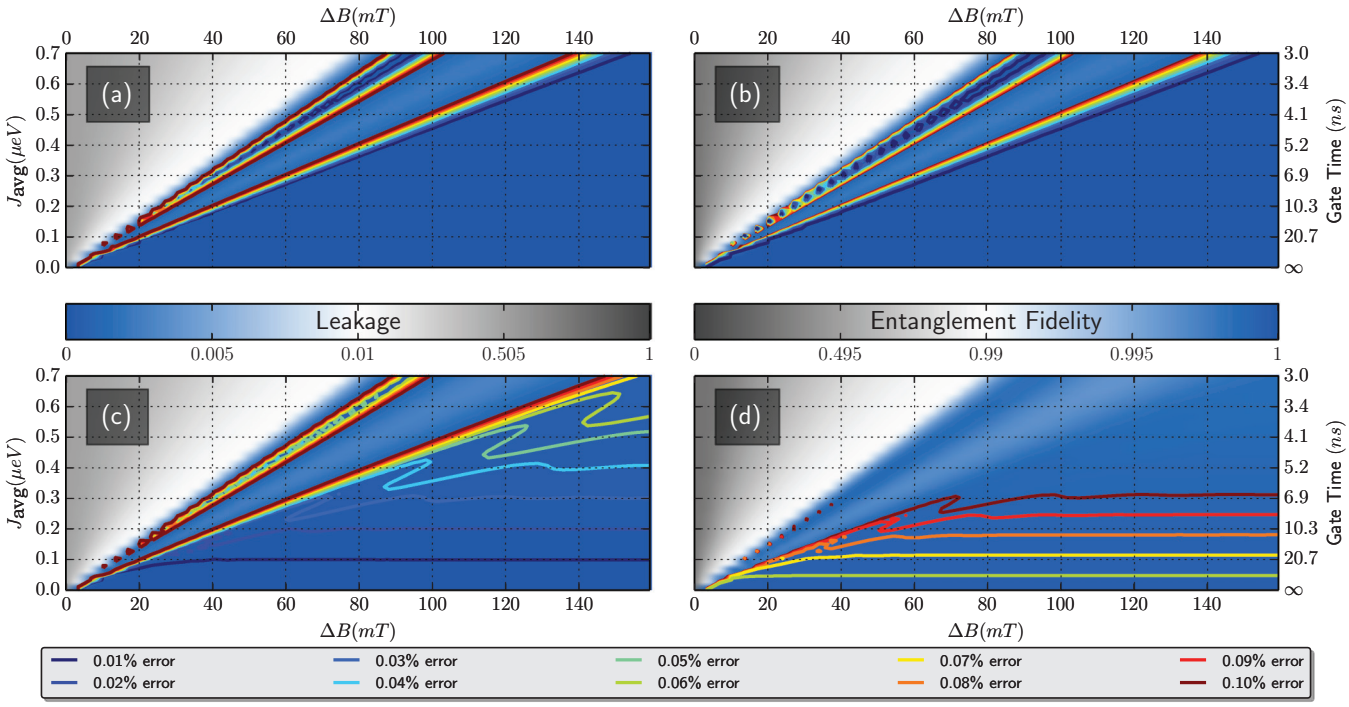

FIG. 5. (Color online) Simulated leakage and entanglement fidelity immediately after a single two-qubit gate operation as a function of J_{avg} and ΔB, with gate time corresponding to each labeled J_{avg} shown on the far right axes. Panels (a) and (c) show the leakage results with and without charge noise respectively, and panels (b) and (d) show the entanglement fidelity results with and without charge noise respectively. The color maps for leakage and entanglement fidelity are shown in the corresponding column, and are chosen such that comparable colors indicate comparable errors. The color maps are white at 1% error, with larger error shown in shades of grey, and lesser error in shades of blue. Contours corresponding to 0.01–0.10% error are drawn at 0.01% intervals.

energy scale, and set to be 200 mT. As described in Sec. IV B, simulations of our gate require us to choose an ansatz for $J(\varepsilon)$, the details of which are not important provided that the dependence matches closely phenomenological results. In these simulations we use $J(\varepsilon) = J_0 \exp(\varepsilon/\varepsilon_D)$, with the free parameters J_0 and ε_D chosen to roughly match the experimental results of Dial and collaborators [24]. In simulations we add a very small negative constant offset to allow for $J(\varepsilon)$ to be exactly zero, which does not significantly affect the results. Also following the prescription of Sec. IV B, we calibrated the noise parameters $\sigma_{\tilde{\varepsilon}}$ and D such that the T_2^* and T_2 times in simulations of single-qubit gates were somewhat typical [24]; specifically, we calibrated $\sigma_{\tilde{\varepsilon}}$ and D such that $T_2^* \approx 100$ ns and $T_2 \approx 1$ μs. We summarize our choice of parameters in Table II.

In Fig. 5 we plot leakage with and without charge noise [Figs. 5(a) and 5(c) respectively], and entanglement fidelity with and without noise [Figs. 5(b) and 5(d) respectively], at the end of a single two-qubit gate operation as a function of the average exchange coupling J_{avg} and interqubit magnetic field gradient ΔB. The gate time corresponding to each value of J_{avg} is labeled on the rightmost axes. We use a segmented color map which goes through white at 1% error, with blue toward 0%, and dark grey toward 100%. Contours corresponding to 0.01–0.10% error are drawn at 0.01% intervals, corresponding to the regime in which fault-tolerant computing starts to become feasible (typically 10^{-2}–10^{-4}) [55]. The positions of the contours on both the leakage and fidelity plots roughly correspond, because $\mathcal{F} \approx 1 - \mathcal{L}_0$ (see Sec. V).

The simulations confirm several important qualities of our gate. The radial nature of the contours from the origin indicates that our gate's leakage is largely predicted by the ratio $J_{\text{avg}}/\mu\Delta B$, as described in Sec. IV A. We also observe the qualitative features anticipated in Sec. V: that charge noise causes the entanglement fidelity to decrease even more quickly than leakage increases due to its being sensitive to phases on the logical subspace [seen in Eq. (6)], that leakage ceases to be the dominant source of error (for any given fidelity) at long enough gate times, and that fidelity increases approximately hyperbolically with gate time (or equivalently, decreases linearly with J_{avg}).

By way of ballpark numbers, we find that our two-qubit gate has fidelities in excess of ~99.9% for gate times longer than around 7 ns and magnetic field gradients of around 80 mT. In this regime, leakage is no longer the dominant source of noise, and gate fidelities are affected by noise in essentially the same way as single-qubit gates, as described in Sec. V. On this basis, we feel that our gate may be well suited for quantum computation using singlet-triplet qubits.

VII. DISCUSSION

In this paper we have analyzed the performance of an exchange-based two-qubit gate for singlet-triplet qubits. Our approach uses a magnetic field gradient to suppress spin-flip transitions that would otherwise lead to leakage errors. We have shown that adiabatic pulses can reduce the leakage probability by several orders of magnitude. We have also investigated the effect of charge noise on the performance of our gate, showing that, by running the gate sufficiently slowly, it is possible to achieve entanglement fidelities that are comparable to those of single-qubit operations. In this limit, we showed that the performance is limited by low-frequency charge noise. Two-qubit gate simulations demonstrated that this regime can be reached using realistic exchange couplings and magnetic field gradients.

The two-qubit gate we have described works whenever there is an effective exchange coupling between the qubits. This could be a direct exchange coupling (as we have envisaged here), or an indirect coupling through an intermediate dot which has recently been shown to generate an effective exchange interaction [38].

The approach of energetically suppressing spin-flip transitions in order to implement two-qubit gates using exchange coupling has application in other qubit architectures; for example, we used a similar approach in our proposal for two-qubit gates for the resonant-exchange qubit [30]. We anticipate that the use of adiabatic pulses will greatly reduce leakage in that scheme also.

ACKNOWLEDGMENTS

We thank S. Bartlett, B. Halperin, D. Loss, C. Marcus, I. Neder, D. Reilly, and M. Rudner for discussions. Research was supported by the Office of the Director of National Intelligence, Intelligence Advanced Research Projects Activity (IARPA), through the Army Research Office Grant No. W911NF-12-1-0354. We acknowledge support from the ARC via the Centre of Excellence in Engineered Quantum Systems (EQuS), Project No. CE110001013.

[1] R. Hanson, J. R. Petta, S. Tarucha, and L. M. K. Vandersypen, Rev. Mod. Phys. **79**, 1217 (2007).
[2] C. Kloeffel and D. Loss, Annu. Rev.: Condens. Matter Phys. **4**, 51 (2013).
[3] D. Loss and D. P. DiVincenzo, Phys. Rev. A **57**, 120 (1998).
[4] D. P. DiVincenzo, Fortschr. Phys. **48**, 771 (2000).
[5] B. M. Maune, M. G. Borselli, B. Huang, T. D. Ladd, P. W. Deelman, K. S. Holabird, A. A. Kiselev, I. Alvarado-Rodriguez, R. S. Ross, A. E. Schmitz *et al.*, Nature (London) **481**, 344 (2012).
[6] J. P. Dehollain, J. T. Muhonen, K. Y. Tan, A. Saraiva, D. N. Jamieson, A. S. Dzurak, and A. Morello, Phys. Rev. Lett. **112**, 236801 (2014).
[7] B. Trauzettel, D. V. Bulaev, D. Loss, and G. Burkard, Nat. Phys. **3**, 192 (2007).
[8] D. V. Bulaev, B. Trauzettel, and D. Loss, Phys. Rev. B **77**, 235301 (2008).
[9] J. R. Petta, A. C. Johnson, J. M. Taylor, E. A. Laird, A. Yacoby, M. D. Lukin, C. M. Marcus, M. P. Hanson, and A. C. Gossard, Science **309**, 2180 (2005).
[10] F. H. L. Koppens, C. Buizert, K. J. Tielrooij, I. T. Vink, K. C. Nowack, T. Meunier, L. P. Kouwenhoven, and L. M. K. Vandersypen, Nature (London) **442**, 766 (2006).
[11] M. Pioro-Ladrière, T. Obata, Y. Tokura, Y.-S. Shin, T. Kubo, K. Yoshida, T. Taniyama, and S. Tarucha, Nat. Phys. **4**, 776 (2008).

[12] T. Obata, M. Pioro-Ladrière, Y. Tokura, Y.-S. Shin, T. Kubo, K. Yoshida, T. Taniyama, and S. Tarucha, Phys. Rev. B **81**, 085317 (2010).
[13] S. Nadj-Perge, S. M. Frolov, E. P. A. M. Bakkers, and L. P. Kouwenhoven, Nature (London) **468**, 1084 (2010).
[14] R. Brunner, Y.-S. Shin, T. Obata, M. Pioro-Ladrière, T. Kubo, K. Yoshida, T. Taniyama, Y. Tokura, and S. Tarucha, Phys. Rev. Lett. **107**, 146801 (2011).
[15] J. Levy, Phys. Rev. Lett. **89**, 147902 (2002).
[16] A. C. Johnson, J. R. Petta, J. M. Taylor, A. Yacoby, M. D. Lukin, C. M. Marcus, M. P. Hanson, and A. C. Gossard, Nature (London) **435**, 925 (2005).
[17] R. Hanson and G. Burkard, Phys. Rev. Lett. **98**, 050502 (2007).
[18] C. Barthel, D. Reilly, C. Marcus, M. Hanson, and A. Gossard, Phys. Rev. Lett. **103**, 160503 (2009).
[19] H. Bluhm, S. Foletti, I. Neder, M. Rudner, D. Mahalu, V. Umansky, and A. Yacoby, Nat. Phys. **7**, 109 (2010).
[20] C. Barthel, J. Medford, H. Bluhm, A. Yacoby, C. Marcus, M. Hanson, and A. Gossard, Phys. Rev. B **85**, 035306 (2012).
[21] M. D. Shulman, O. E. Dial, S. P. Harvey, H. Bluhm, V. Umansky, and A. Yacoby, Science **336**, 202 (2012).
[22] D. Stepanenko, M. Rudner, B. I. Halperin, and D. Loss, Phys. Rev. B **85**, 075416 (2012).
[23] J. Klinovaja, D. Stepanenko, B. I. Halperin, and D. Loss, Phys. Rev. B **86**, 085423 (2012).
[24] O. E. Dial, M. D. Shulman, S. P. Harvey, H. Bluhm, V. Umansky, and A. Yacoby, Phys. Rev. Lett. **110**, 146804 (2013).
[25] D. P. DiVincenzo, D. Bacon, J. Kempe, G. Burkard, and K. B. Whaley, Nature (London) **408**, 339 (2000).
[26] E. A. Laird, J. M. Taylor, D. P. DiVincenzo, C. M. Marcus, M. P. Hanson, and A. C. Gossard, Phys. Rev. B **82**, 075403 (2010).
[27] L. Gaudreau, G. Granger, A. Kam, G. C. Aers, S. A. Studenikin, P. Zawadzki, M. Pioro-Ladrière, Z. R. Wasilewski, and A. S. Sachrajda, Nat. Phys. **8**, 54 (2012).
[28] J. Medford, J. Beil, J. M. Taylor, E. I. Rashba, H. Lu, A. C. Gossard, and C. M. Marcus, Phys. Rev. Lett. **111**, 050501 (2013).
[29] J. Medford, J. Beil, J. M. Taylor, S. D. Bartlett, A. C. Doherty, E. I. Rashba, D. P. DiVincenzo, H. Lu, A. C. Gossard, and C. M. Marcus, Nat. Nanotechnol. **8**, 654 (2013).
[30] A. C. Doherty and M. P. Wardrop, Phys. Rev. Lett. **111**, 050503 (2013).
[31] S. Foletti, H. Bluhm, D. Mahalu, V. Umansky, and A. Yacoby, Nat. Phys. **5**, 903 (2009).
[32] M. Gullans, J. J. Krich, J. M. Taylor, H. Bluhm, B. I. Halperin, C. M. Marcus, M. Stopa, A. Yacoby, and M. D. Lukin, Phys. Rev. Lett. **104**, 226807 (2010).
[33] R. P. G. McNeil, R. J. Schneble, M. Kataoka, C. J. B. Ford, T. Kasama, R. E. Dunin-Borkowski, J. M. Feinberg, R. J. Harrison, C. H. W. Barnes, D. H. Y. Tse *et al.*, Nano Lett. **10**, 1549 (2010).
[34] T. Takakura, M. Pioro-Ladrière, T. Obata, Y.-S. Shin, R. Brunner, K. Yoshida, T. Taniyama, and S. Tarucha, Appl. Phys. Lett. **97**, 212104 (2010).
[35] S. Lloyd, Phys. Rev. Lett. **75**, 346 (1995).
[36] I. van Weperen, B. D. Armstrong, E. A. Laird, J. Medford, C. M. Marcus, M. P. Hanson, and A. C. Gossard, Phys. Rev. Lett. **107**, 030506 (2011).
[37] J. G. Coello, A. Bayat, S. Bose, J. H. Jefferson, and C. E. Creffield, Phys. Rev. Lett. **105**, 080502 (2010).
[38] S. Mehl, H. Bluhm, and D. P. DiVincenzo, Phys. Rev. B **90**, 045404 (2014).
[39] R. Li, X. Hu, and J. Q. You, Phys. Rev. B **86**, 205306 (2012).
[40] J. P. Kestner, X. Wang, L. S. Bishop, E. Barnes, and S. Das Sarma, Phys. Rev. Lett. **110**, 140502 (2013).
[41] X. Wang, L. S. Bishop, E. Barnes, J. P. Kestner, and S. DasSarma, Phys. Rev. A **89**, 022310 (2014).
[42] J. M. Taylor, V. Srinivasa, and J. Medford, Phys. Rev. Lett. **111**, 050502 (2013).
[43] J. M. Taylor, H.-A. Engel, W. Dür, A. Yacoby, C. M. Marcus, P. Zoller, and M. D. Lukin, Nat. Phys. **1**, 177 (2005).
[44] L. Trifunovic, O. Dial, M. Trif, J. R. Wootton, R. Abebe, A. Yacoby, and D. Loss, Phys. Rev. X **2**, 011006 (2012).
[45] L. DiCarlo, J. M. Chow, J. M. Gambetta, L. S. Bishop, B. R. Johnson, D. I. Schuster, J. Majer, A. Blais, L. Frunzio, S. M. Girvin *et al.*, Nature (London) **460**, 240 (2009).
[46] See Supplemental Material at http://link.aps.org/supplemental/10.1103/PhysRevB.90.045418 for an analytical description of the energy level structure of two singlet-triplet qubit systems, the details of our adiabatic perturbation theory predictions and fidelity calculations, and a derivation of the fidelity-leakage relation.
[47] D. J. Reilly, J. M. Taylor, J. R. Petta, C. M. Marcus, M. P. Hanson, and A. C. Gossard, Science **321**, 817 (2008).
[48] W. A. Coish, D. Loss, E. A. Yuzbashyan, and B. L. Altshuler, J. Appl. Phys. **101**, 081715 (2007).
[49] C. De Grandi and A. Polkovnikov, in *Quantum Quenching, Annealing and Computation*, Lecture Notes in Physics, edited by A. K. Chandra, A. Das, and B. K. Chakrabarti, Vol. 802 (Springer, Berlin/Heidelberg, 2010), pp. 75–114.
[50] H. M. Wiseman and G. J. Milburn, *Quantum Measurement and Control* (Cambridge University Press, Cambridge, UK, 2010).
[51] E. Paladino, Y. M. Galperin, G. Falci, and B. L. Altshuler, Rev. Mod. Phys. **86**, 361 (2014).
[52] M. A. Nielsen and I. L. Chuang, *Quantum Computation and Quantum Information (Cambridge Series on Information and the Natural Sciences)*, 10th ed. (Cambridge University Press, Cambridge, UK, 2010).
[53] M. Horodecki, P. Horodecki, and R. Horodecki, Phys. Rev. A **60**, 1888 (1999).
[54] M. A. Nielsen, Phys. Lett. A **303**, 249 (2002).
[55] D. Gottesman, arXiv:quant-ph/0701112.